

Stretching and twisting of the DNA duplexes in coarse grained dynamical models.

Szymon Niewieczyza and Marek Cieplak

*Institute of Physics Polish Academy of Science,
Al. Lotników 32/48, 02-668 Warsaw, Poland*

October 30, 2018

Abstract

Three coarse-grained models of the double-stranded DNA are proposed and compared in the context of mechanical manipulation such as twisting and various schemes of stretching. The models differ in the number of effective beads (between two and five) representing each nucleotide. They all show similar behavior and, in particular, lead to a torque-force phase diagrams qualitatively consistent with experiments and all-atom simulations.

1 Introduction

Manipulation of large biomolecules by means of atomic force microscopy, optical tweezers, and other nanotechnological devices is playing an increasingly growing role in elucidating mechanisms of biologically relevant processes [1, 2, 3]. The dynamical data obtained through mechanical manipulation usually requires theoretical interpretation that can be reached through numerical simulations. This need is especially apparent when dealing with proteins (see, e.g., [4]) because of their strongly inhomogeneous network of interactions between the amino acids. The inhomogeneity results, for instance, in a protein-dependent pattern of peaks when the force of resistance to pulling at constant speed is plotted against elongation (see, e.g. [5, 6, 7, 8]).

All-atom simulations have contributed to understanding of the large conformational changes in proteins induced by the mechanical manipulation (see e.g. [9, 10, 11]). However, such simulations are inherently limited by the time scales and system sizes that can be studied. One way out is to accelerate the modeled processes by orders of magnitude relative to their experimental realizations which may, undesirably, distort the physics involved. Another way is to use coarse grained models. These models can also be applied to other processes involving large conformational changes such as folding or thermal unfolding of biomolecules. They may also find applications in studies of systems which are much larger in size.

In this paper, we focus on coarse grained models describing the double stranded DNA (dsDNA). The simplest coarse graining scheme involves treating dsDNA as a polymer endowed with a local stiffness [12]. The resulting model seems to be appropriate in studies of stretching at high temperatures, when the entropic effects dominate, and in studies of phenomena related to fluid flow and the hydrodynamic interactions [13]. The corresponding characteristic dimension in this model can be measured by the Kuhn length or the hydrodynamic radius. The typical values of these parameters are of order 106 and 77 nm [13] respectively which encompasses more than 200 distances (of 0.4 nm) between successive pairs of nucleotides in the dsDNA. This level of coarse graining is thus too crude to be useful when describing mechanical manipulation of the system where nanometric features are detectable. Here, we discuss coarse grained models with structures that are resolved at the level of a single nucleotide.

There are a variety of possible ways to manipulate the DNA duplex. The ones that we consider in this paper are schematically represented in Figure 1. Unzipping, whether at constant speed or at constant force, corresponds to scheme A in this Figure. The unzipping process

involves breaking of one hydrogen bond at a time resulting in a force, F , of order 13-15 pN, that rapidly undulates with the amplitude of order 1 pN as the pulling distance, d , is increased [14, 15]. The force pattern has also been found to depend on the pulling speed, v_p , weakly [14], but would be expected to depend on temperature, T , more substantially. Even though the variations in the $F - d$ patterns when pulling at constant speed take place on the nucleotidic length scales, their interpretation in terms of the specifics of the sequence is difficult because of the noise due to thermal fluctuations. Recently, Baldazzi et. al. [16] has suggested, however, that if instead the mechanical unzipping is performed at constant force then Bayesian methods of the corresponding sequence prediction should be nearly error-free. Methods for extracting kinetic information from constant force experiments have been discussed recently in the context of DNA unzipping in a nanopore [17].

Schemes B and C involve stretching at the opposite ends of the duplex. The two schemes employ distinct mechanisms of resistance to stretching. Mechanism B involves shear which is responsible for generation of the strongest force clamps in biomolecules [4] and the maximum force obtained depends on the number of the bonds that are sheared simultaneously. Mechanism C, on the other hand, leads to localized unravelling and generates a size-independent force. When using micropipettes, as in the experiment by Cluzel et al. [18], one probably combines schemes B and C. The resulting $F - d$ pattern has three stages: one starts off with a long period of a nearly constant force, after which there is a steady increase (in the 120 pN range) which finally is followed by a sudden drop to zero. A similar pattern of behavior arises in simulations involving anisotropic pressure [19] (these studies have been performed for a dsDNA with about 10 pairs of nucleotides).

Still another way of manipulating the dsDNA has been employed by Oroszi et al. [20] and it involves applying a torque, G . Wereszczynski and Andricioaei [21] have generalized it still further, in their all-atom simulations, by considering a simultaneous application of a force and torque, as shown in scheme D in Figure 1. They have predicted existence of a rich phase diagram of possible structures on the $F - G$ plane. There have been experimental studies involving torque produced in an optical trap [22, 20, 23]. Bryant et. al. [22] have found that the torque needed to transform the B-DNA conformation into the left-hand twisted L-DNA form is $G = -9.6$ pN nm (the negative sign indicates twisting against the native sense of turn in the dsDNA), while to transform it further into the Pauling-like (P-DNA) form the required torque is 34 pN nm. They have also observed that by pulling

the dsDNA molecule with the force of about 65 pN one induces a transition from the B-DNA into the S-DNA form which is 60% longer than the B-DNA.

In this paper, we construct three variants of the nucleotide-based coarse grained dynamical models of the DNA duplex. The coarse graining method introduces several effective objects, referred here as beads, that represent a single nucleotide. The models differ primarily by the number of beads involved. We compare the workings of the three models for a 22-base-pair system, or shorter, and use them to elucidate the mechanisms of rupture in processes corresponding to schemes A through D. One conclusion of our studies is that even though various dynamical details differ between the models, all of them can be considered adequate and ready to be applied to larger systems. In particular, all of the coarse grained models studied lead to a transition of the usual right-hand-twisted B-dsDNA form to the L-dsDNA form and to the P-DNA form on application of an appropriate torque.

2 An overview of the models used

Physical properties of the DNA double helix are quite distinct [24] compared to other biomolecules. Its strong stiffness comes from the braided nature of its structure combined with the presence of the base stacking interactions. Furthermore, the phosphate groups in the DNA backbone carry substantial electric charges. All of these features are employed by the cell's machinery in the processes of copying, transcribing and packaging of the DNA. For example, helicases which unwind the double helix to provide single-stranded templates for polymerases, have evolved as motors that are capable of moving along the torsionally constrained DNA molecules. Topoisomerases break and reconnect the DNA to relieve a torsional strain that accumulates ahead of the replication fork. Finally, the DNA-binding proteins get docked to the DNA by means of guidance mechanisms which seem to be primarily electrostatic in nature.

Our models address the mechanical properties of the dsDNA and do not aim at determining the electrostatic potential outside of the duplex. The models are built in analogy to the Go-like models of proteins, especially in the specific implementation proposed in refs.[25, 27, 28, 4]. In the case of proteins, the model represents the system by its C^α atoms which are tethered together by harmonic interactions. The native contacts, such as the hydrogen bonds, are described by the Lennard-Jones potentials. The Langevin overdamped thermostat with random forces mimics fluctuational effects of the solvent. 61 other variants of this basic model of a protein are discussed and compared

in ref. [29].

The dsDNA has a simpler elastic structure than proteins since a pair of nucleotides can bind only in two ways: either by forming two (A-T) or three (G-C) hydrogen bonds. When trying to build a coarse grained model for a DNA one is first inclined to assign a single bead to a nucleotide and to locate it at the phosphorus (P) atom. This may be acceptable for a single strand DNA, provided the local chain stiffness terms are included. However, for the dsDNA this procedure would lead to a distance of 17 Å between the P atoms in a hydrogen bonded pair of the nucleotides. Such a relatively large distance would introduce too much mechanical instability in the model but appears to be adequate to study conformational changes in dsDNA nanocircles and submicron-sized plasmids with torsional stress [30]. A more detailed approach, denoted here as model I, involves representing the A and T nucleotides by four beads and the G and C nucleotides by five beads. One of the beads represents the phosphate group, another the sugar group, and the remaining beads participate in formation of either two or three hydrogen bonds, depending on the specificity. The hydrogen bond interactions are represented by the effective Lennard-Jones potentials and other bonds, being structural in nature, are described by the harmonic potentials with large elastic constants. The schematic construction of this model is shown in Figure 2.

More simplified approaches involve reduction in the number of beads representing each nucleotide. In a model denoted here as model II, we mimic the ribose-phosphate groups by one bead and the base by another bead as illustrated by the top of Figure 3. In this model, the distinction between the A:T and G:C pairing interactions comes not through introduction of separate contacts for each hydrogen bond but through adjustment of the amplitude of the effective base-base Lennard-Jones potential by a factor of 2 or 3 respectively.

In between models I and II there is another model, denoted here as model III, that has been introduced by Knott et al. [31] in the context of the salt induced melting. Model III involves three beads as illustrated in the bottom part of Figure 3. The beads represent the phosphate, sugar, and base groups correspondingly. In model III, the backbone chain of one strand is constructed by linking the sugar group to the P atom on the same nucleotide and to the P atom on a preceding nucleotide. Thus the backbone chain has the appearance of a zigzag line. In contrast, in models I and II, the backbone chain is formed by tethering the consecutive P atoms.

As a model system we consider the structure coded as 119D in the Protein Data Bank which has been determined by Leonard and Hunter [32]. It corresponds to the sequence 5'-

D(CGTAGATCTACGTAGATCTACG)-3'. The ground state conformations of this system as captured by the three models are shown in Figure 4. Longer structures can be obtained, for instance, by repeating this basic unit, or by constructing a synthetic sequence-dependent structure that makes use of average geometrical parameters associated with a single base pair.

3 Model I: the 4- or 5-bead description

We start by introducing three different types of beads, p, h, and b as illustrated in Figure 2. The p-beads are meant to represent the backbone which is made of the phosphate groups. The p-bead is placed at the position of the C4* atom in the molecule of ribose. This placement achieves two goals. First, it represents the DNA phosphate chain by the p-beads. Second, it locates the p-bead close to the base beads. The C4* atom is the ribose ring atom that is closest to the phosphate group. The h-beads represent the 'head' atoms which may act either as donors or as acceptors in the hydrogen bonds. In the C nucleotides, the h-beads are located on the O2, N3, and N4 atoms of the bases. In the G nucleotides, – on the O6, N1, and N2 atoms. Finally, in the A and T nucleotides – on the N6, N1, and N3, O4 atoms respectively. The h-beads are linked to their 'bases', i.e. to the supporting b-beads. In the native state, the b-beads are located half-way between the p-bead and the center of mass of the h-beads at each nucleotide. The overall scheme results in about 4- to 5-fold reduction in the number of the degrees of freedoms compared to the all-atom approach.

In Table 1 we provide the Cartesian coordinates of the beads that define the model. Knowledge of these coordinates should allow for a generation of a synthetic dsDNA based on the sequence. The coordinates have been obtained by making averages of the geometric parameters in the PDB structure corresponding to the basic sequence studied.

The p-beads are tethered into two separate chains and thus form two backbones. The tethering is accomplished through the elastic potential

$$V_{i,i+1}^{pp} = K_b \cdot (\vec{r}_{p_i} - \vec{r}_{p_{i+1}} - d_{p_i p_{i+1}})^2 , \quad (1)$$

where index i enumerates consecutive nucleotides and $d_{p_i p_{i+1}}$ are the distances between the consecutive p-beads in the native state. These distances vary from bead to bead. Their mean is equal to 5.8 Å and the standard deviation is close to 0.3Å. The mean geometrical parameters cited in this description can be used in a general sequence-dependent construction of a synthetic dsDNA structure. The elastic constant is

taken to be equal to $K_b = 50 \epsilon \text{\AA}^{-2}$, where ϵ is the energy scale corresponding to the internucleotidic hydrogen bonds, as defined below.

The steric constraints of the DNA sugar-phosphate backbone are represented by the following two potentials for the bond and dihedral angles of p-beads' backbone.

$$V^B = \sum_{i=\mathcal{N}_1}^{\mathcal{N}-2} K_\theta (\theta_i - \theta_{0i})^2 , \quad (2)$$

$$V^D = \sum_{i=1}^{\mathcal{N}-3} [K_\phi^1 (1 + \cos(\phi_i - \phi_{0i})) + K_\phi^3 (1 + \cos 3(\phi_i - \phi_{0i}))] . \quad (3)$$

The bond angle θ_i is measured between the $p_i - p_{i+1}$ and $p_{i+1} - p_{i+2}$ bonds, and the dihedral angle ϕ_i is an angle between two planes: one of them is determined by the $p_i - p_{i+1}$ and $p_{i+1} - p_{i+2}$ bonds, and the second one by the $p_{i+1} - p_{i+2}$ and $p_{i+2} - p_{i+3}$ bonds, the subscript 0 indicates the native values, \mathcal{N} denotes the number of nucleotides in one chain. We take $K_\theta = 20\epsilon/(\text{rad})^2$, $K_\phi^1 = 1.0\epsilon$, $K_\phi^3 = 0.5\epsilon$ in analogy to ref. [33].

All of the interbead interactions within one nucleotide are taken to be harmonic so that the corresponding potentials read

$$V_{i,i}^{\nu\mu} = \sum_{\nu,\mu} K_b \cdot (\vec{r}_{\mu_i} - \vec{r}_{\nu_i} - d_{\mu_i\nu_i})^2 , \quad (4)$$

where the indices ν and μ label beads belonging to the i 'th nucleotide. The equilibrium distances $d_{\mu\nu}$ take values as in the native structure and they range from $2.3 \pm 0.1 \text{\AA}$ for the neighboring h-beads (according to notation in Figure 2, pairs: h_{1j} - h_{2j} and h_{2j} - h_{3j}) to $3.6 \pm 0.7 \text{\AA}$ between the b-bead and h-beads.

The h-beads on one chain are capable of making hydrogen-bond contacts with the h-beads on the opposite chain. In the simplest version, we follow the prescription used previously for proteins and describe these contacts by the Lennard-Jones potential

$$V_{i,j}^{hh} = 4\epsilon \left[\left(\frac{\sigma_{h_i h_j}}{r_{h_i h_j}} \right)^{12} - \left(\frac{\sigma_{h_i h_j}}{r_{h_i h_j}} \right)^6 \right] , \quad (5)$$

where i and j are the paired residues and $r_{h_i h_j} = |\mathbf{r}_{h_i} - \mathbf{r}_{h_j}|$. The parameters $\sigma_{h_i h_j}$ are chosen so that each contact in the native conformation is stabilized in the minimum of the potential. Essentially, $\sigma_{h_i h_j} = 2^{-1/6} d_{h_i h_j}$. The value of $d_{h_i h_j}$, the distance between h-beads making bond, is equal to $2.66 \pm 0.14 \text{\AA}$. For proteins, the choice of the form of the contact potential has turned out to be of much less importance than the correct determination of the contact map [29].

The stacking interactions between consecutive b-beads in each chain are also accounted for by the Lennard-Jones interactions:

$$V_{i,i+1}^{bb} = 4\epsilon\left[\left(\frac{\sigma_{b_i b_{i+1}}}{r_{b_i b_{i+1}}}\right)^{12} - \left(\frac{\sigma_{b_i b_{i+1}}}{r_{b_i b_{i+1}}}\right)^6\right] . \quad (6)$$

The distance between the stacking pairs of the b-beads is 4.43 ± 0.42 Å in the native structure.

All of the interactions discussed above arise in the native state. However, distorted conformations may lead to new interactions. In the spirit of the Go-like models, we describe these by purely repulsive potentials (the Lennard-Jones potentials which are cut at the minimum and shifted). The hard sphere diameters of the h- b- and p-beads are taken to be equal to 2.0 Å, 3.4 Å, and 6.0 Å respectively. The large effective size of the p-bead prevents the chains from crossing and self-crossing.

All beads are endowed with the same mass, m , and the equation of motion of each is described by the Langevin equation

$$m\ddot{\vec{r}} = -\gamma(\dot{\vec{r}}) + \vec{F}^c + \vec{\Gamma} , \quad (7)$$

which provides thermostating and mimics dynamical effects of the solvent. Here \vec{r} is the position of the bead, \vec{F}^c is the net force on it due to potentials, γ is the friction coefficient, and $\vec{\Gamma}$ is a white noise term with the dispersion of $\sqrt{2\gamma k_B T}$, where k_B is the Boltzmann constant and T is the temperature. The dimensionless temperature, $k_B T/\epsilon$, will be denoted by \tilde{T} . The friction coefficient γ is equal to $2m/\tau$ where τ is a characteristic time scale. The dynamics are meant to be overdamped so the characteristic time scale corresponds to a diffusional passage of a molecular distance (~ 3 Å) and is thus of order 1 ns. For small damping, τ would correspond to time scale of (ballistic) oscillations in the Lennard-Jones well which is significantly shorter. The equations of motion are solved by the fifth order predictor-corrector scheme [34].

As the average value of energy for hydrogen bond interaction in dsDNA we chose 0.6 kcal/mole, while in [35] it was chosen around 0.5-0.7 kcal/mole, and in [31]: 0.66 kcal/mole. On average, 2.5 hydrogen bonds are created between the bases in dsDNA. Hence the total average energy of interaction between paired bases in the DNA helix is about 1.5 kcal/mole in our models. This choice is consistent with $\tilde{T} = 0.4$ corresponding to $T=300$ K. The corresponding unit of the force, $\epsilon/\text{Å}$ should be then of order 100 pN. In the entropic limit, the hydrogen bond potentials matter much less than the thermal fluctuations. In our model, this starts to happen at \tilde{T} of about 0.5 – 0.6.

4 Model II: the 2-bead model description

In the 2-bead model, we consider beads denoted by p and b at each nucleotide as shown in Figure 3. The p-beads are placed in positions of the C4* atom and mimic the phosphate-ribose chain of the DNA molecule. The harmonic tethering potential, as well as the bond and the dihedral angle potentials are introduced in analogy to model I. The b-bead in each nucleotide is placed in the geometrical center of the base. The absence of the h-beads of model I is compensated by introducing hydrogen-bond-like interactions between the b-beads. The average Cartesian coordinates of the model beads are provided in Table 1. In order to distinguish between the A:T and G:C pairs in the DNA sequence, we strengthen the amplitude of the corresponding Lennard-Jones potential by the factor of 2 or 3 respectively. The stacking potential, between the neighbouring b-beads along each DNA is described as in model I. The hard sphere diameters of the beads remain defined as in model I. Average value of the bead mass is $m = 162$ g/mole and the distance between the beads that make effective hydrogen bonds is 5.5 ± 0.8 . We have determined that the persistence length in model II at $\tilde{T} = 0.4$ is about 50 nm.

5 Model III: the 3-bead description

Model III, introduced in ref. [31] and shown schematically in Figure 3 provides a 3-bead description. It differs from model II primarily as a result of a different treatment of the backbone chain. In model II, the sugar and phosphate groups of the same nucleotide are represented by one bead, whereas in model III the two groups are represented by separate beads so that the backbone chain is formed by connecting sugar bead (s) of one nucleotide to the phosphate bead of the nucleotide that follows in the sequence.

The distinction between the phosphate and sugar groups is important in this model because it facilitates introduction of electrostatic charges on the phosphate beads. The charges are introduced to describe interactions of the DNA with ions in the solvent but they also affect the p-p distances through the resulting Coulombic repulsion. The corresponding potential is given by $V_{elec,ij} = \sum \frac{q_i q_j}{4\pi\epsilon_0\epsilon r_{ij}} e^{-r_{ij}/\kappa_D}$, where κ_D is the Debye constant, and its value depends on the ionic strength of the solution. For standard ionic strengths, κ_D ranges from 11 to 15 Å (eg. when $[\text{Na}^{2+}] = 50\text{mM}$, one obtains $\kappa_D = 13.6\text{Å}$). Here, we do not take this term into account, as its effect on the p-p distances

is minor and because our focus is on mechanical manipulations and not on the effects resulting from variations of the ionic strength.

Other potentials used in this model are analogous to those used in models I and II. The exception is the base pairing potential. We describe it by the effective Lennard-Jones potential whereas Knotts et al. [31] by the 10-12 potential

$$V^{bp} = \sum_{\text{base pairs}} 4\epsilon_{bp} \left[5 \left(\frac{\sigma_{bp}}{r_{ij}} \right)^{12} - 6 \left(\frac{\sigma_{bp}}{r_{ij}} \right)^{10} \right] , \quad (8)$$

where ϵ_{bp} depends on the type of base pair (AT or GC, while $\epsilon_{GC} = 3/2 \cdot \epsilon_{GC}$), and σ_{bp} is around 2.9 Å for all paired bases.

Hyeon and Thirumalai [35] have recently considered a model of the RNA hairpin in which every nucleotide is represented by three beads which correspond to the phosphate, sugar and base groups which is analogous to model III of the double helix and to the model of Knotts et al. [31]. Similar to ref. [31], the Debye-Hueckel potential between the phosphate beads is introduced to account for screening by condensed counterions and for the hydration effects. However, there are differences pertaining to the nonbonded potentials. In addition to the base pairing potential, Hyeon and Thirumalai introduce a possibility of stacking interactions between the base beads. Such interactions do not arise between the successive nucleotides, but may arise in, e.g., the head of an RNA hairpin. These stacking interactions are responsible for existence of the more complicated conformations, like the hairpin, that the RNA may adopt. As to the base pairing potential, Hyeon and Thirumalai take the Lennard-Jones potential without making a distinction between the number of the hydrogen bonds involved. It affects the base beads which are within the distance of 7 Å and the corresponding depth of the potential is 1.8 kcal/mole. Non-native base bead interactions are repulsive and correspond to the energy parameter of 1.0 kcal/mole.

Another simple model of the DNA has been recently proposed by Ouldridge et al. [36] in the context of self-assembly of DNA nanostructures in which the twisting character of the individual strands is disregarded. In this model, every nucleotide is represented by a softly repulsive sphere of diameter $l=6.3$ Å and by another smaller sphere attached (nearly) rigidly to the center of the repulsive sphere at a distance of $0.3l$ away from it and perpendicularly to the backbone. The smaller sphere provides a center of attraction to another small sphere and thus plays the role of a base in the DNA strand. Four types of the base site are considered and the Lennard-Jones attraction links the complementary bases. Additionally, the model incorporates a monomer-to-monomer bending energy to provide stiffness. In the

ground state, two strands run parallel to each other like in a β sheet in proteins.

Throughout the paper, we use the open square, solid square, and triangle symbols to denote results corresponding to models I, II, and III respectively.

A convenient way to characterize the unravelling process is by providing the distance at which a given contact breaks down for the last time. A contact is said to be broken if the corresponding distance exceeds 1.5 times the length parameter σ in the Lennard-Jones potential associated with the contact. For models II and III, where there is only one connection between paired bases (through the b-beads) the contacts are labelled by the nucleotide number, l , as counted from the side that is being pulled. In the case of model I, where each nucleotide can participate in either 2 or 3 contacts, the graphical representation uses the ordinates of $l - 0.1$ and $l + 0.1$ for residues A and T whereas it involves $l - 0.2$, l and $l + 0.2$ for residues G and C.

6 Unzipping at constant speed in scheme A

The stretching scheme A shown in Figure 1 leads to the unzipping process in which the hydrogen bonds break by starting from the end that is being pulled. These bonds are enumerated by the index l which is being counted from the pulling end. Figure 5 shows the force vs. displacement patterns at $T=0$ for two different values of the pulling velocity, v_p , of 0.05 and 0.005 $\text{\AA}/\tau$ and for the three models discussed. At temperatures that are lower than 0.12 ϵ/k_B , the $F - d$ patterns are qualitatively similar to the ones shown in Figure 5 in the sense that the individual force peaks can usually be related to unravelling of specific base pairs in the DNA sequence.

In the initial stages of unravelling, all bonds that exist in the system get adjusted to some extent and it is only later on that the unravelling process becomes more site specific. This is well seen in model I for $d < 50 \text{\AA}$, especially for the higher pulling speed, where all force peaks are quite similar. In the other two models, this transient distance is much shorter because the number of the adjustable bonds is smaller. However, after this transient stage is passed, one can read off the pair sequence of the double helix from the $F - d$ patterns easily because the higher peaks arise due to breaking of the G:C bonds. The smaller the pulling speed the crisper the recognition of the sequence.

At $\tilde{T} = 0.4$, we observe the peaks with the maximal value of 0.39 ϵ/A (which corresponds to about 40 pN) - Figure 6. These values are

about 20 pN higher than the experimental results [14, 15], where for $v_p = 200$ nm/s one obtains peaks of 18-20 pN

The bottom panels of Figures 5 and 6 show the scenario diagrams arising in scheme A. At sufficiently low temperatures the zipping process is seen to be proceeding linearly in time with minor differences in slopes between the models. At higher temperatures, like for $T = 0.4\epsilon/\text{\AA}$ in model I, the scenario diagram data points acquire a curved appearance. This indicates that the thermal fluctuations rupture bonds at the idle (and not anchored) end of the dsDNA before the mechanical unzipping process gets to them.

For $T = 0$ the force peaks have values of 1-2 $\epsilon/\text{\AA}$ in all three models. On increasing the temperature, the peaks and $\langle F \rangle$, i.e. the force averaged over the duration of the full unravelling process (till F drops to 0), get lowered in a monotonic fashion, as shown in Figure 7, which presents the results for unravelling with velocities $v_p = 0.05 \text{\AA}/\tau$ and $v_p = 0.005 \text{\AA}/\tau$. At the higher temperatures, model II yields the biggest mean forces, independent of the pulling speeds. Models I and III yield comparable mean forces at these temperatures and it depends on the velocity which one is stronger of the two.

With lowering the unravelling velocity, the calculated average forces decrease. In Figure 8 we present the average forces for model I for three different unravelling velocities. There is a big decrease of the $\langle F \rangle$ between the $v_p = 0.05 \text{\AA}/\tau$ and $v_p = 0.01 \text{\AA}/\tau$, while the results obtained for $v_p = 0.01 \text{\AA}/\tau$ and $v_p = 0.005 \text{\AA}/\tau$ are close to each other. Generally, the smaller the velocity, the smaller the $\langle F \rangle$ values. The similar dependencies are observed for models II and III. Around $T = 0.3 \epsilon/\text{\AA}$ the rapid decrease in $\langle F \rangle$ switches to a nearly constant behavior at higher temperatures.

7 Stretching at constant speed in scheme B

The B-type stretching has an entirely different nature than the A-type one. In this scheme, only one chain undergoes active stretching and this effect in turn influences the companion chain through the hydrogen-bond contacts. Figure 9 illustrates the mechanics of this kind of manipulation. The snapshots (as obtained within model II) show that a full extension of one chain results in a substantial distortion of the other chain. Furthermore, F depends on d in a monotonic fashion. There are no force peaks even at $T=0$. The $F - d$ curves for models I and II coincide and a bigger force arises faster than in model III because of a more direct transmission of tension between the p-beads.

The scenario diagrams also look distinct compared to scheme A and in a way which is more sensitive to T . At $T=0$ many contacts are broken nearly simultaneously. At finite temperatures, the contacts at the extremities get ruptured before unravelling of the contacts in the middle in each of the models studied. The higher the T , the earlier particular contacts break down. We have observed insignificant dependence of the rupture distances on the pulling velocity. The whole process results in unravelling both of the hydrogen-bond and of the stacking contacts.

8 Stretching at constant speed in scheme C

In the C-type stretching, one chain is made to slide along its companion until the two chains separate as shown in Figure 10. The $F - d$ curves display a major peak which is an order of magnitude larger than the force peaks observed in scheme A in all of the three models studied. The emergence of this major peak is due to an increasingly cooperative resistance to manipulation of many contacts that are sheared simultaneously. Once the rupture takes place, the force drops down to the level corresponding merely to the thermal noise. The cooperation level appears to be the greatest in model III, followed by model II. In each of the models, the rupture of all contacts is nearly simultaneous.

The maximal force peak dependence on temperature shown in Figure 11 for two velocities indicated is similar to what was observed for $\langle F \rangle$ in scheme A, especially at low temperatures. Models II and III yields are found to yield comparable forces which are also noticeably larger than in model I except at the low temperature end. For the C-type stretching, the dependence on the stretching velocity is weak as demonstrated in Figure 12. The inset demonstrates that the dependence is nearly logarithmic.

9 Stretching at constant force and constant torque in scheme D

We now consider the tensile and torsional manipulations of the dsDNA and focus on the determination of the corresponding force-torque phase diagram.

We introduce the torsional stress of the dsDNA molecule in the following way. At one end of the molecule we choose two vectors defining the plane. First vector is defined by the positions of the

extreme p-beads at the chosen end of the dsDNA. The second vector defining the plane is a cross product of the first vector and the dsDNA axis (which is defined by the midpoints of the extreme beads on both ends of DNA molecule). In the plane constructed in the way described above we add two more beads as shown in Figure 13 so that a square frame of four beads is formed. All beads in this frame are connected by the springs as in other structural bonds. The extreme beads on the other end of the molecule are anchored at their starting positions.

The torsion is applied to the DNA molecule by application of a force to each of the four beads in the square frame. The torque is perpendicular to the frame. The torsion is considered positive if it agrees with the sense of the twist in the double helix in the B form and it is considered negative otherwise. The stretching force F is a resultant force applied to all of the four beads in the frame and along the dsDNA axis.

We first consider model II at two temperatures: 0.2 and 0.4 $\epsilon/\text{\AA}$. The results are presented in the phase diagram in the Figure 14. The boundaries of the phases are approximate and are quite similar in both models. These phase diagrams are also similar in appearance to those established experimentally [22, 20, 23] and theoretically [39, 22].

We start from the dsDNA B-form structure and observe the transitions into other phases of the DNA structure. At $T = 0.4 \epsilon/\text{\AA}$, the DNA transforms into the L-form under the torque G of around -1.5ϵ . At the lower temperature, this transformation occurs for G of around 1.8-2.0 ϵ . The simulations which lead to the L-form with the value of the torque being close to this limiting value may last for up to 15000 τ . This time becomes significantly shorter for larger values of G .

The S-form of the DNA was experimentally characterised by overstretching of the dsDNA molecule by about 60%. In models I and II the elongation of the system leads to tightening of the bonds between p-beads along the chains, which finally leads to significant increase in the applied force. Thus the S-form region in the dsDNA phase diagram corresponds to structures in which the backbone forms the straight line, without imposing the condition of 60% overstretching. In $T = 0.4 \epsilon/\text{\AA}$ such structures occur while there is applied the force of 0.5 $\epsilon/\text{\AA}$. For lower temperature there is needed a bit larger force for about 0.05-0.1 $\epsilon/\text{\AA}$. The above values were obtained for applied torque G of 1.5 ϵ and 1.7 ϵ respectively for temperatures of 0.4 ϵ and 0.2 ϵ .

The Pauling form is obtained when both the stretching force and the positive twisting torque are large. The smallest value of force needed to transform the system into the DNA P-form is 0.25 $\epsilon/\text{\AA}$, while the torque applied must be of value around 5.0 ϵ . For larger stretching forces, G decreases to 2.1 ϵ at $F = 1.5 \epsilon/\text{\AA}$. In the P-form

form, the p-beads come closer together while the remaining beads (b and h) become exposed and face out of the helix.

10 Stretching at constant angular speed in scheme D

In order to study stretching at a constant angular speed, we anchor the bottom beads and attach two frames to the top. Each of these frames is as described in the previous section and they coincide initially. The beads in one frame are connected to their twins by elastic springs. As the outer frame rotates at a constant angular speed, these springs get stretched and impose a twist on the inner frame which is glued to the DNA. This construct facilitates determination of the resistive torque as it is accomplished by monitoring stretching of the interframe springs.

Figure 15 shows the torque of resistance to twisting as a function of the angle of rotation of the outer frame. Two magnitudes of the angular speed, ω , are used, $0.00014 \frac{1}{\tau}$ and $0.00069 \frac{1}{\tau}$, which differ by the factor of 5. We also probe two senses of the twisting: agreeing with the helical twist ($\omega > 0$) or opposing it ($\omega < 0$). The former leads to overtwisting and an indefinite growth in the resistive torque due to an increasing infringement of the steric constraints. The latter results in unwinding and in a transition from the B-form to the L-form. The results clearly depend on the twisting speed. In particular, the average torques are 0.319ϵ and 0.890ϵ for the smaller and faster negative angular speeds respectively. The peaks in the torque result from the distortions, but no contacts get ruptured when one infers about it from the distance-based criterion.

11 Conclusions

The coarse-grained models of the dsDNA discussed here allow for studies of features at the level of a single nucleotide. These models are found to be fairly equivalent and indicate that sequence-specific events can be observed in mechanical manipulations performed at low temperatures. However, this capability becomes borderline around the room temperature.

Nevertheless the models proposed here should be useful when studying DNA-protein complexes and when assisting nanotechnological DNA assembly processes theoretically. Examples of such processes are described in references [40, 41, 42].

Many fruitfull discussions with P. Szymczak are appreciated. This work has been supported by the grant N N202 0852 33 from the Ministry of Science and Higher Education in Poland.

References

- [1] C. Bustamante, Z. Bryant, and S. B. Smith, *Nature* **421**, 423-426 (2003).
- [2] D. A. Koster, V. Croquette, C. Dekker, S. Shuman, and N. H. Dekker, *Nature* **434**, 671-674 (2005).
- [3] J. F. Marko, *Proc. Natl. Acad. Sci. (USA)* **94**, 11770-11772 (1997).
- [4] J. I. Sułkowska and M. Cieplak, *J. Phys.: Cond. Mat.* **19**, 283201 (2007).
- [5] M. Rief, M. Gautel, F. Oesterhelt, J. M. Fernandez, and H. E. Gaub, *Science* **276** 1109-1112 (1997).
- [6] S. B. Fowler, R. B. Best, J. L. Toca Herrera, T. J. Rutherford and A. Steward, E. Paci, M. Karplus, and J. Clarke, *J. Mol. Biol.* **322**, 841-849 (2002).
- [7] G. Yang, C. Cecconi, W. A. Baase, I. R. Vetter, W. A. Breyer, J. A. Haack, B. W. Matthews, F. W. Dahlquist, and C. Bustamante *Proc. Natl. Acad. Sci. (USA)* **97**, 139-144 (2000).
- [8] M. Carrion-Vazquez, A. F. Oberhauser, T. E. Fisher, P. E. Marszalek, H. Li, and J. M. Fernandez, *Prog. Biophys. Mol. Biol.* **74**, 63-91 (2000).
- [9] H. Lu and K. Schulten, *Chemical Physics* **247** 141-153 (1999).
- [10] E. Paci and M. Karplus, *Proc. Natl. Acad. Sci. (USA)* **97**, 6521-6526 (2000).
- [11] G. Pabon and L. M. Amzel, *Biophys. J.* **91**, 467-472 (2006).
- [12] F. Marko and E. D. Siggia, *Macromolecules* **27**, 981 (1994); *ibid* **28**, 8759 (1995).
- [13] R. M. Jendrejack, J. J. de Pablo, and M. D. Graham, *J. Chem. Phys.* **116** 7752-7759 (2002).
- [14] U. Bockelmann, B. Essevaz-Roulet, and F. Heslot, *Phys. Rev. Lett.* **79**, 4489-4492 (1997).
- [15] U. Bockelmann, Ph. Thomen, B. Essevaz-Roulet, V. Viasnoff, and F. Heslot, *Biophys. J.* **82**, 1537-1553 (2002).
- [16] V. Baldazzi, S. Cocco, E. Marinari, R. Monasson, *Phys. Rev. Lett.* **96**, 128102 (2006).
- [17] O. K. Dudko, G. Hummer, and A. Szabo, *Proc. Natl. Acad. Sci. (USA)* **105**, 15755-15760 (2008).
- [18] P. Cluzel, A. Lebrun, C. Heller, R. Lavery, J.-L. Viovy, D. Chate-nay, and F. Caron, *Science* **271**, 792-794 (1996).

- [19] B. Luan and A. Aksimentiev, Phys. Rev. Lett. **101**, 118101 (2008).
- [20] L. Oroszi, P. Galajda, H. Kirei, S. Bottka, and P. Ormos, Phys. Rev. Lett. **97** 058301 (2006).
- [21] J. Wereszczynski and I. Andricioaei, Proc. Natl. Acad. Sci. (USA) **103**, 16200-16205 (2006).
- [22] Z. Bryant, M. D. Stone, J. Gore, S. B. Smith, N. R. Cozzarelli, and C. Bustamante, Nature **424**, 338-341 (2003).
- [23] J. F. Allemand, D. Bensimon, R. Lavery, and V. Croquette, Proc. Natl. Acad. Sci. (USA) **95**, 14152-14157 (1998).
- [24] B. Albert, D. Bray, J. Lewis, M. Raff, K. Roberts, and J. D. Watson, *Molecular Biology of the Cell*, third edition, Garland Publishing, New York (1994).
- [25] M. Cieplak and T. X. Hoang, Biophys. J. **84**, 475-488 (2003).
- [26] M. Cieplak, T. X. Hoang, and M. O. Robbins, Proteins **49**, 114-124 (2002).
- [27] M. Cieplak, T. X. Hoang, and M. O. Robbins, Proteins **56**, 285-297 (2004).
- [28] J. I. Kwiecińska and M. Cieplak, J. Phys.: Cond. Mat. **17**, S1565-S1580 (2005).
- [29] J. I. Sułkowska and M. Cieplak, Biophys. J. **95**, 3174-3191 (2008).
- [30] F. Trovato and V. Tozzini, J. Phys. Chem. B **112**, 13197-13200 (2008).
- [31] T. A. Knotts IV, N. Rathore, D. C. Schwartz, J. J. de Pablo J. Chem. Phys. **126**, 84901 (2007).
- [32] G. A. Leonard and W. N. Hunter, J. Mol. Biol. **234**, 198-208 (1993).
- [33] C. Clementi, H. Nymeyer, and J. N. Onuchic, J. Mol. Biol. **298**, 937 (2000).
- [34] M. P. Allen and D. J. Tildesley, *Computer Simulation of Liquids* (Oxford University Press, New York, 1987).
- [35] C. Hyeon and D. Thirumalai, Proc. Natl. Acad. Sci. (USA) **102**, 6789-6794 (2005).
- [36] T. E. Ouldridge, I. G. Johnston, A. A. Louis and J. P. K. Doye, J. Chem. Phys. (in press)
- [37] N. K. Voulgarakis, A. Redondo, A. R. Bishop, and K. Ø. Rasmussen, Phys. Rev. Lett. **96**, 248101 (2006).

- [38] M. Cieplak and T. X. Hoang, *J. Chem. Phys.* **113**, 8319-8328 (2001).
- [39] A. Sarkar, J. F. Léger, D. Chatenay, and J. F. Marko, *Phys. Rev. E* **63**, 051903 (2001).
- [40] N. C. Seeman, *Nature* **421**, 427-430 (2003).
- [41] J. C. Mitchell, J. R. Harris, J. Malo, J. Bath, and A. J. Turberfield, *JACS* **126**, 16342-16343 (2004).
- [42] R. P. Goodman, I. A. T. Schaap, C. F. Tardin, C. M. Erben, R. M. Berry, C. F. Schmidt, and A. J. Turberfield, *Science* **310**, 1661-1665 (2005).

<i>Site</i>	<i>Coordinates</i>		
	<i>x</i>	<i>y</i>	<i>z</i>
<i>MODEL I</i>			
<i>p</i>	-7.039	-2.284	-0.492
<i>b (A)</i>	-3.841	-0.516	0.110
<i>h1(A)</i>	-0.498	0.194	0.286
<i>h2(A)</i>	-0.829	2.308	1.138
<i>b (T)</i>	-4.439	-0.293	-0.489
<i>h1(T)</i>	-2.026	0.614	-0.256
<i>h2(T)</i>	-1.692	2.782	-0.717
<i>b (G)</i>	-3.737	-0.997	-0.186
<i>h1(G)</i>	-0.793	2.423	0.731
<i>h2(G)</i>	-0.449	0.300	0.131
<i>h3(G)</i>	-0.005	-1.851	-0.500
<i>b (C)</i>	-4.603	-0.802	-0.163
<i>h1(C)</i>	-1.768	2.928	-0.103
<i>h2(C)</i>	-2.146	0.665	0.178
<i>h3(C)</i>	-2.524	-1.552	0.428
<i>MODEL II</i>			
<i>p</i>	-7.039	-2.284	-0.492
<i>b (A)</i>	-2.443	0.261	0.832
<i>b (T)</i>	-3.197	1.046	-0.351
<i>b (G)</i>	-2.183	0.230	0.468
<i>b (C)</i>	-3.153	0.825	0.139

Table 1: Cartesian coordinates of the beads in models I and II of the ds-DNA. The coordinates depend on the identity of a nucleotide. The following description shows how to generate the DNA double helix for an arbitrary sequence. For the nucleotide, which is placed in the $(n + 1)$ -th position in the first strand, coordinates of the related beads can be obtained through the following transformation: $x(n + 1) = x\cos(n 36^\circ) - y\sin(n 36^\circ)$, $y(n + 1) = x\sin(n 36^\circ) + y\cos(n 36^\circ)$, $z(n + 1) = z + n3.4$, where x , y and z denote the starting coordinates as listed in the table. This transformations involve rotation around the z axis by 36° , and a shift by 3.4 \AA along the z axis. The second strand in the helix is constructed in a similar way, but the initial coordinates have to be transformed from (x,y,z) into $(-x,y,-z)$ for every bead belonging to the first nucleotide of the second strand. Then one applies the prior transition to generate the positions of the sites belonging to nucleotide paired with $(i + 1)$ -th nucleotide in the first strand. A similar construction for model III is presented in ref. [31].

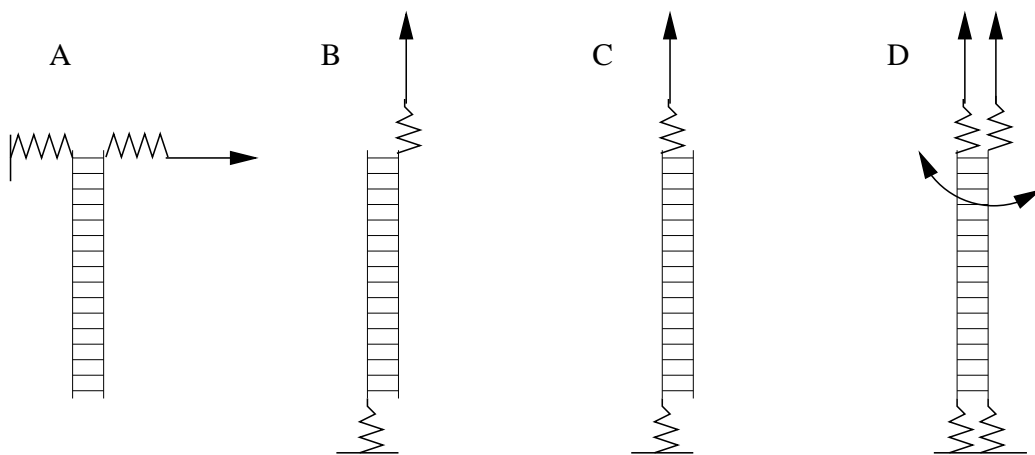
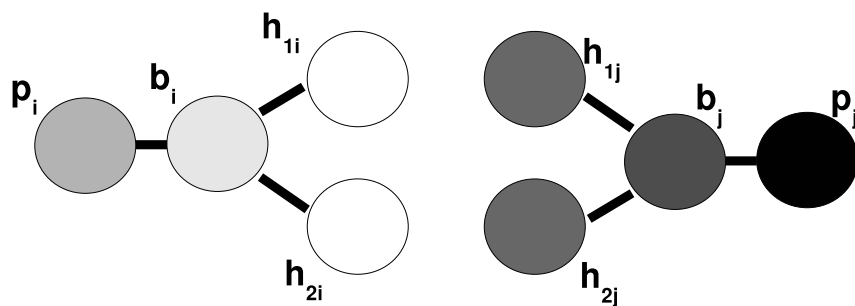


Figure 1: Four possibilities of manipulation of the DNA double helix.

MODEL I

2 hydrogen bonds



3 hydrogen bonds

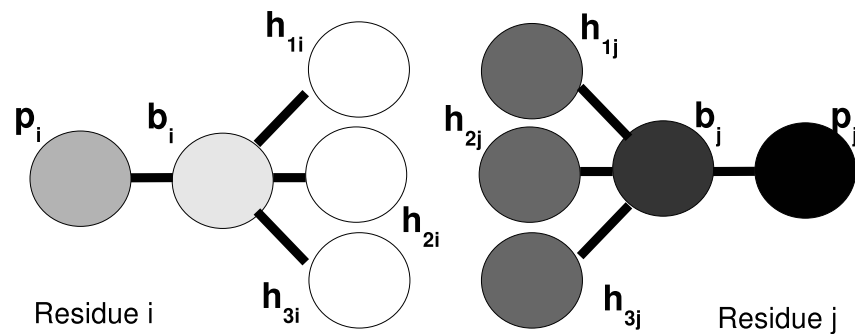
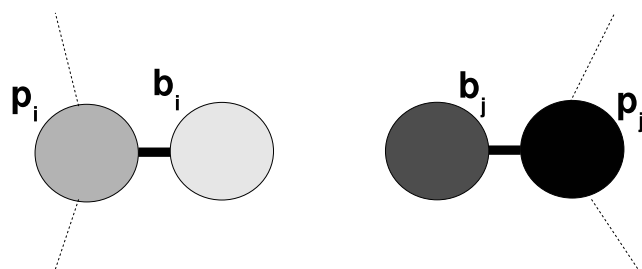


Figure 2: A schematic representation of model I of the dsDNA. It shows formation of 2 and 3 hydrogen bonds.

MODEL II



MODEL III

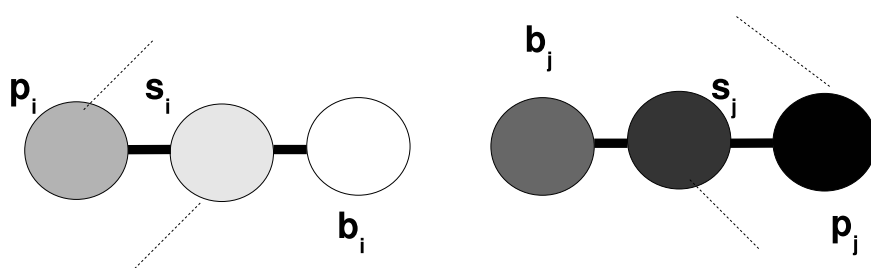


Figure 3: A schematic representation of models II and III. The thin lines indicate the way the backbone chains are constructed.

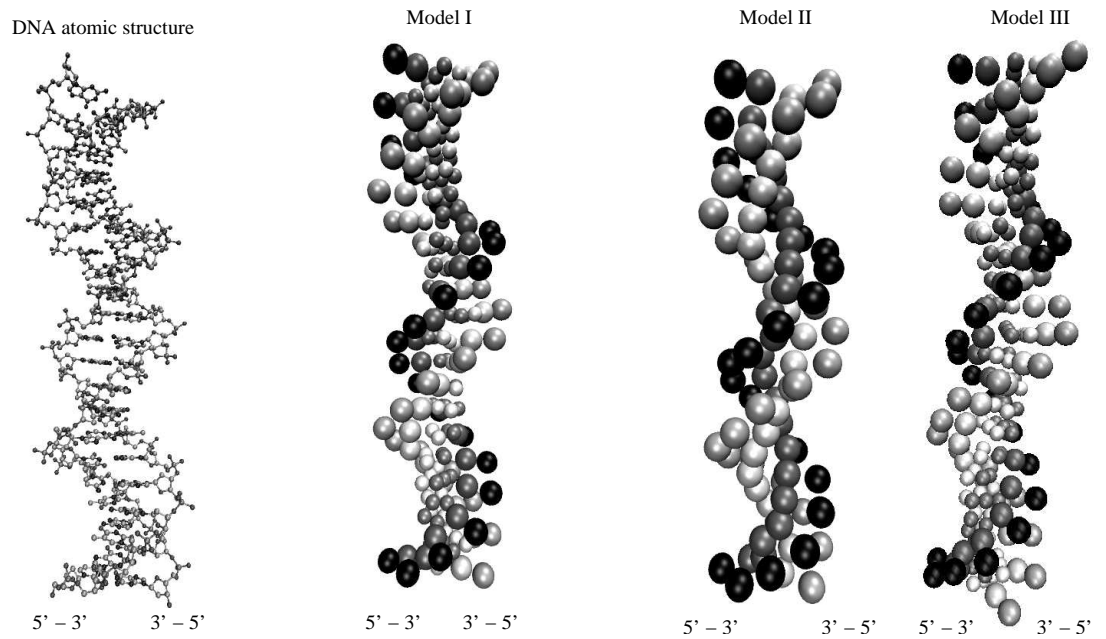


Figure 4: The atomic representation of the 119D dsDNA structure is shown on the left. The remaining panels show the corresponding coarse grained representations considered in this paper.

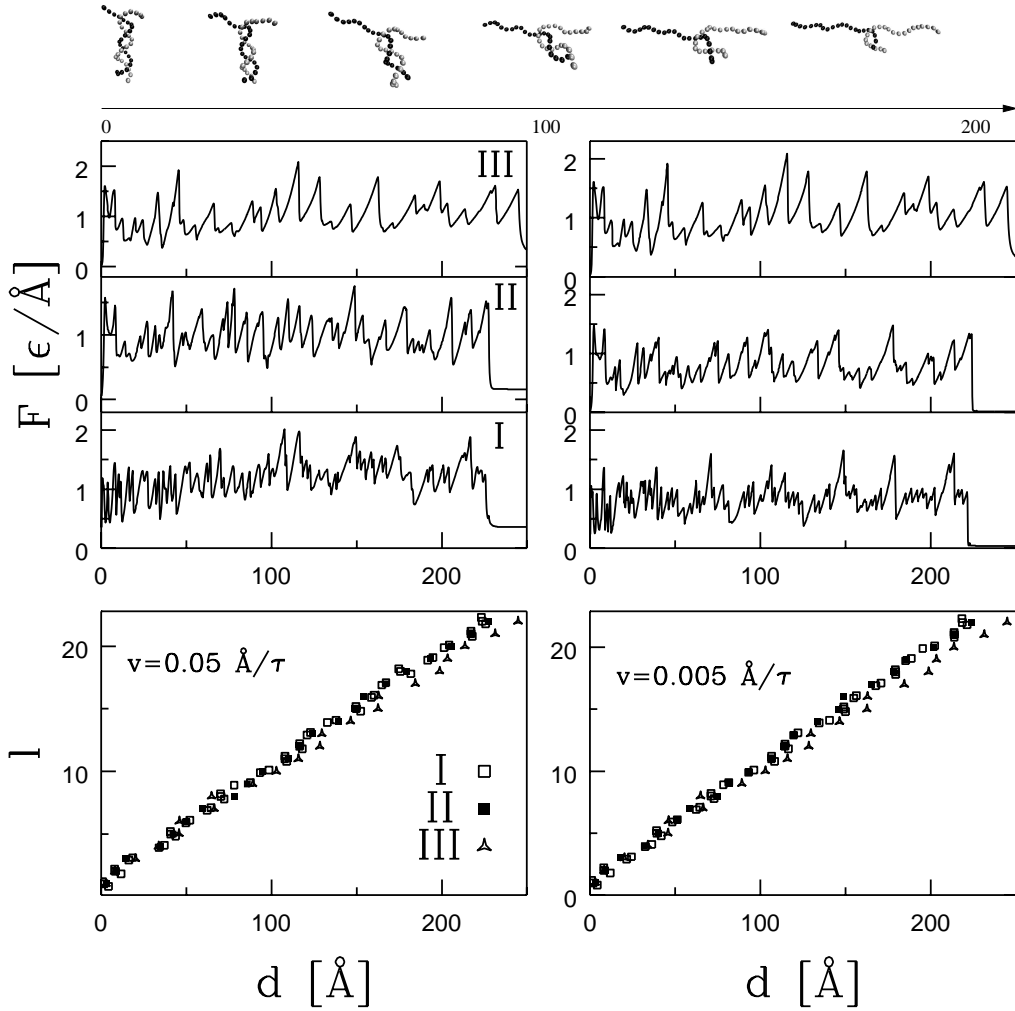


Figure 5: The A-type stretching at $T = 0$. The snapshots at the top show subsequent conformations of the pulled dsDNA in model II for $v_p = 0.05 \text{ \AA}/\tau$. The panels below on the left correspond to $v_p = 0.05 \text{ \AA}/\tau$ and those on the right to $v_p = 0.005 \text{ \AA}/\tau$. The middle panels show the $F - d$ curves for the three models as indicated. At the end of the process, the two chains get fully separated and the force drops to 0. The bottom panels show the corresponding scenarios of unfolding.

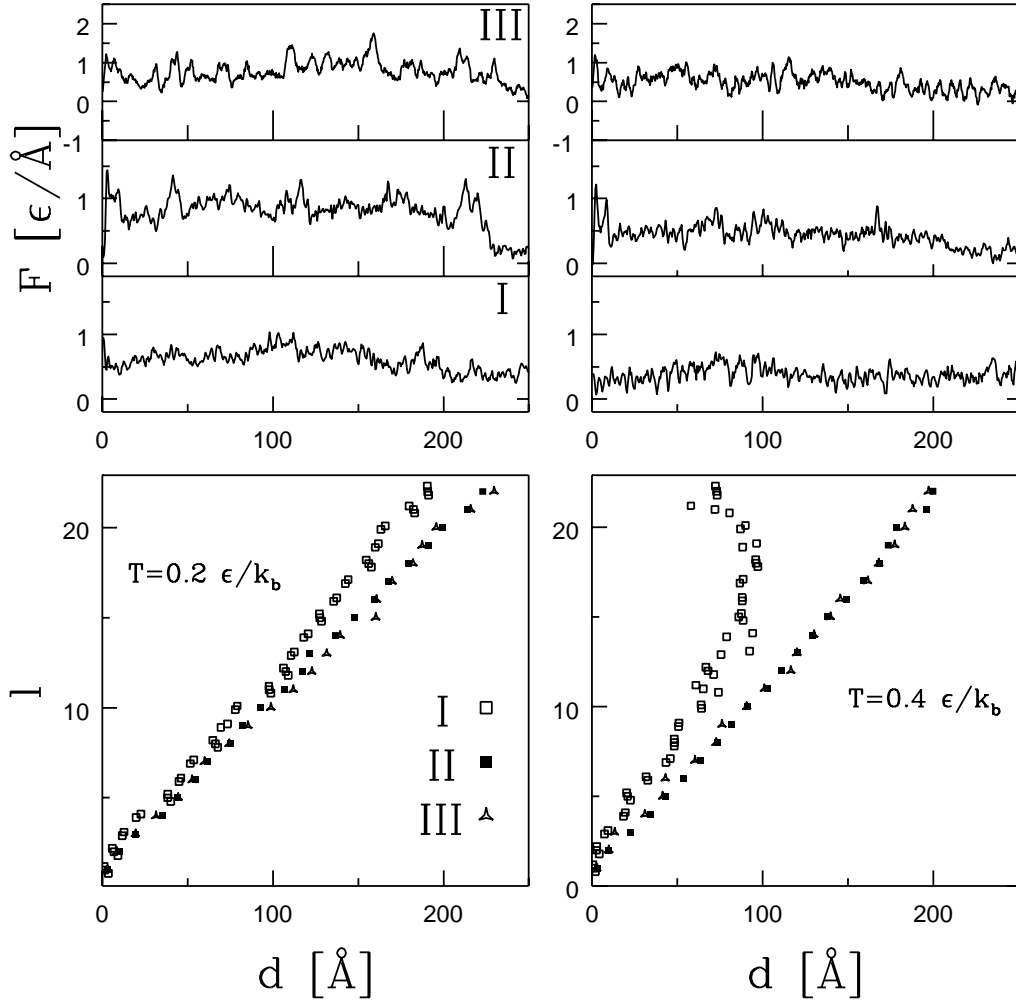


Figure 6: Stretching in the A-type mode at $T = 0.2\epsilon/k_B$ (panels on the left) and at $T = 0.4\epsilon/k_B$ (the panels on the right). The pulling velocity is $0.05 \text{ \AA}/\tau$.

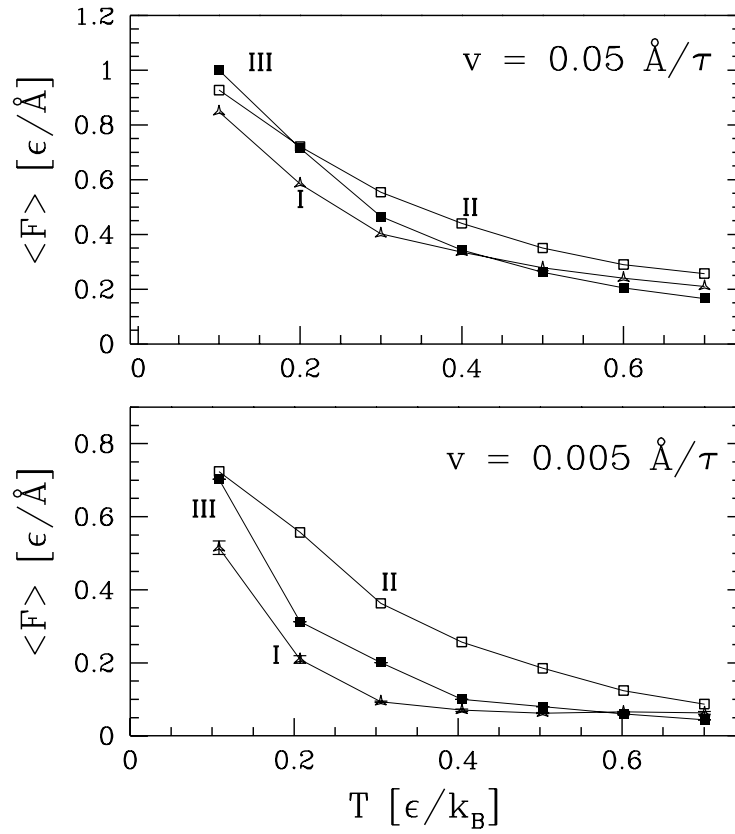


Figure 7: The average force arising during the A-type stretching at $v_p=0.05 \text{\AA}/\tau$ and at $v_p=0.005 \text{\AA}/\tau$ as a function of T for the three models.

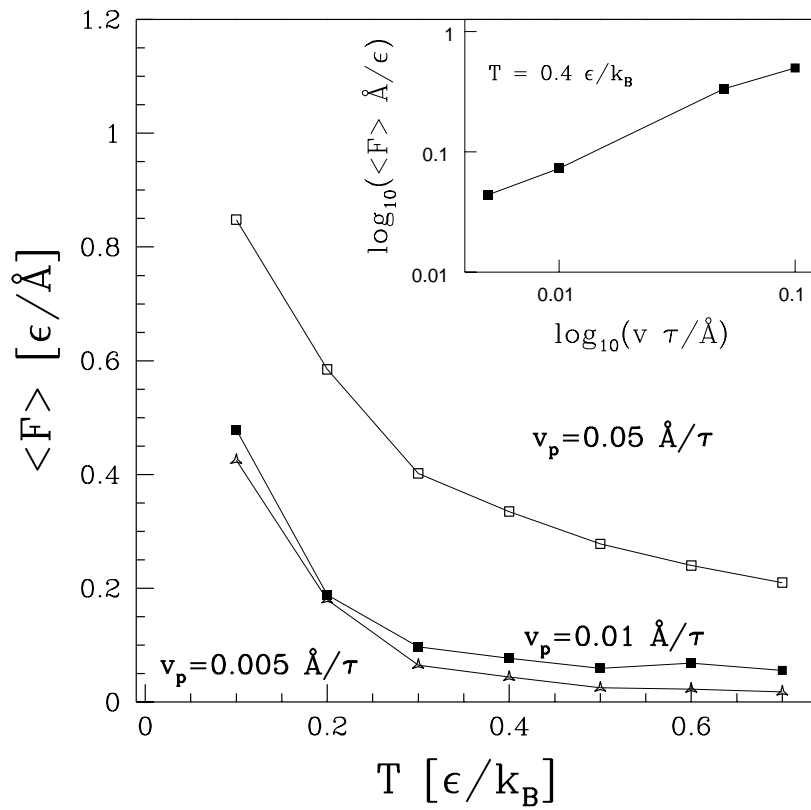


Figure 8: The average force arising during the A-type stretching for three different unravelling velocities in model I. The inset shows the log-log plot of $\langle F \rangle$ vs. v_p .

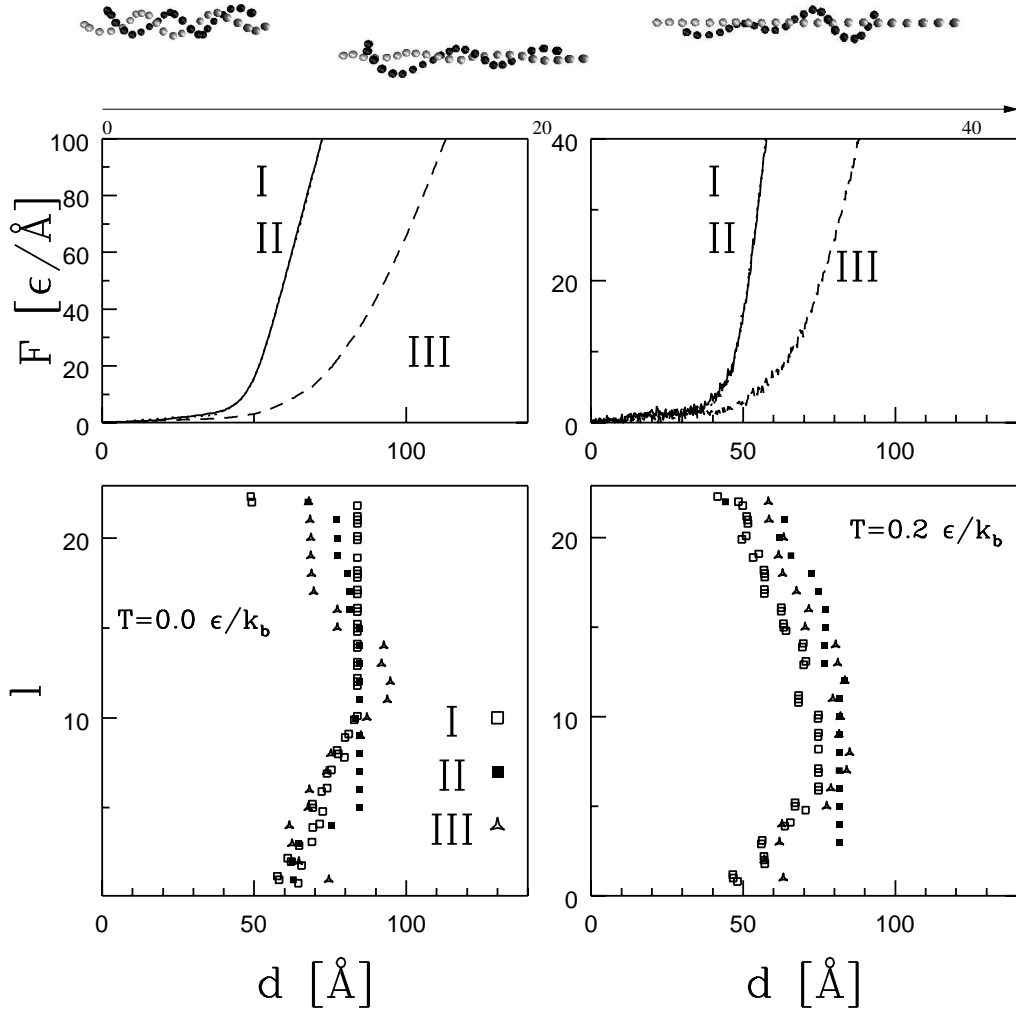


Figure 9: The B-type stretching for $v_p=0.05 \text{ \AA}/\tau$ at two different temperatures for the three models. The panels on the left represent the results corresponding to $T = 0$, and the results shown on the right panels correspond to $T = 0.2\epsilon/k_B$. The snapshots presented at the top show conformations during the stretching process of model II at $T = 0.0$.

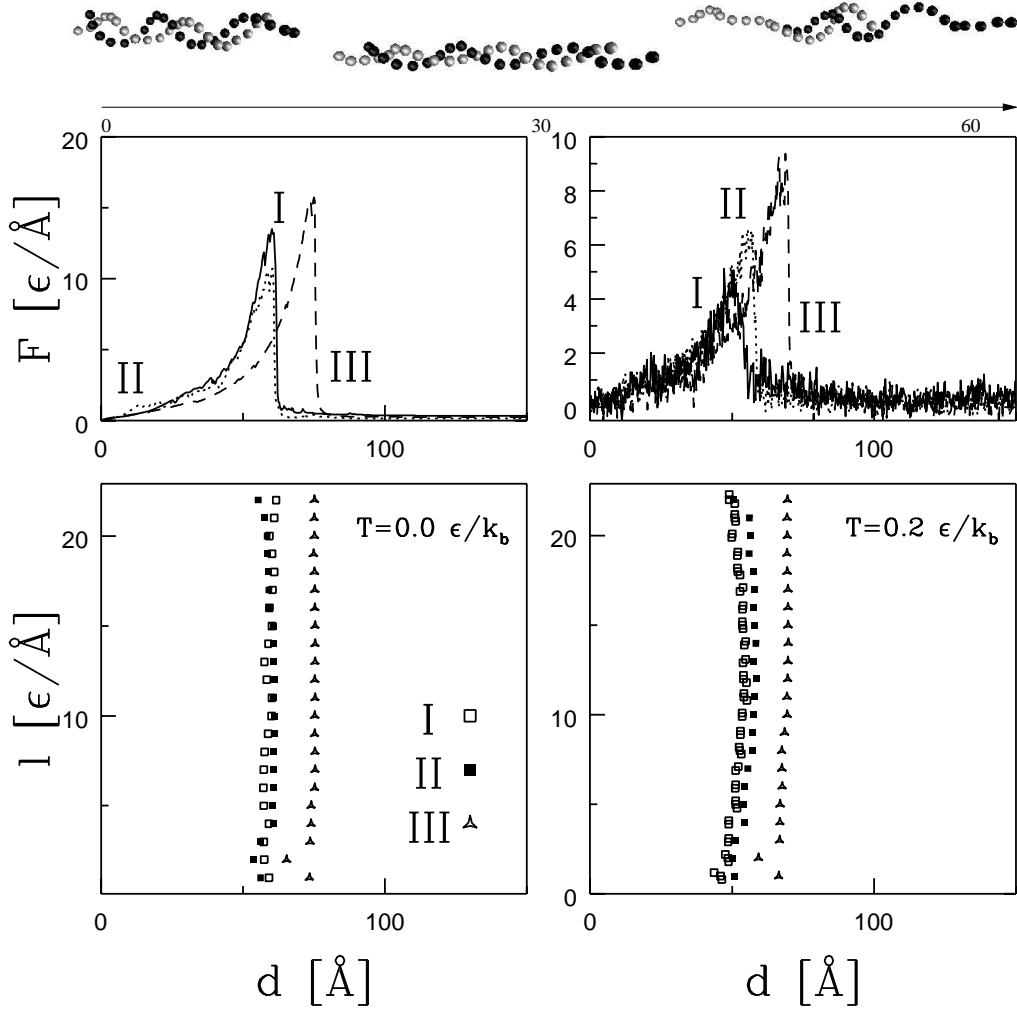


Figure 10: The C-type stretching for $v_p=0.05 \text{ \AA}/\tau$ at two different temperatures for the three models. The panels on the left represent the results corresponding to $T = 0$, and the results shown on the right panels correspond to $T = 0.2\epsilon/k_B$. The snapshots presented at the top show conformations during the stretching process of model II at $T = 0$.

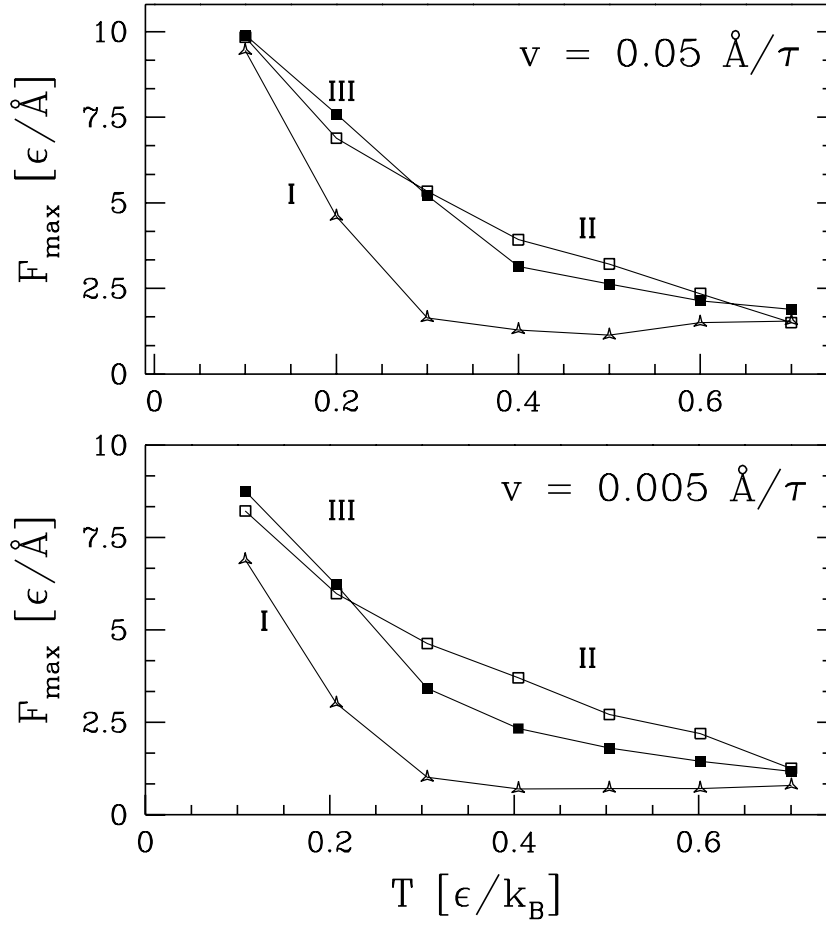


Figure 11: The maximal force for the C-type stretching for $v_p=0.05 \text{ \AA}/\tau$ and for $v_p=0.005 \text{ \AA}/\tau$ as a function of temperature for the three models.

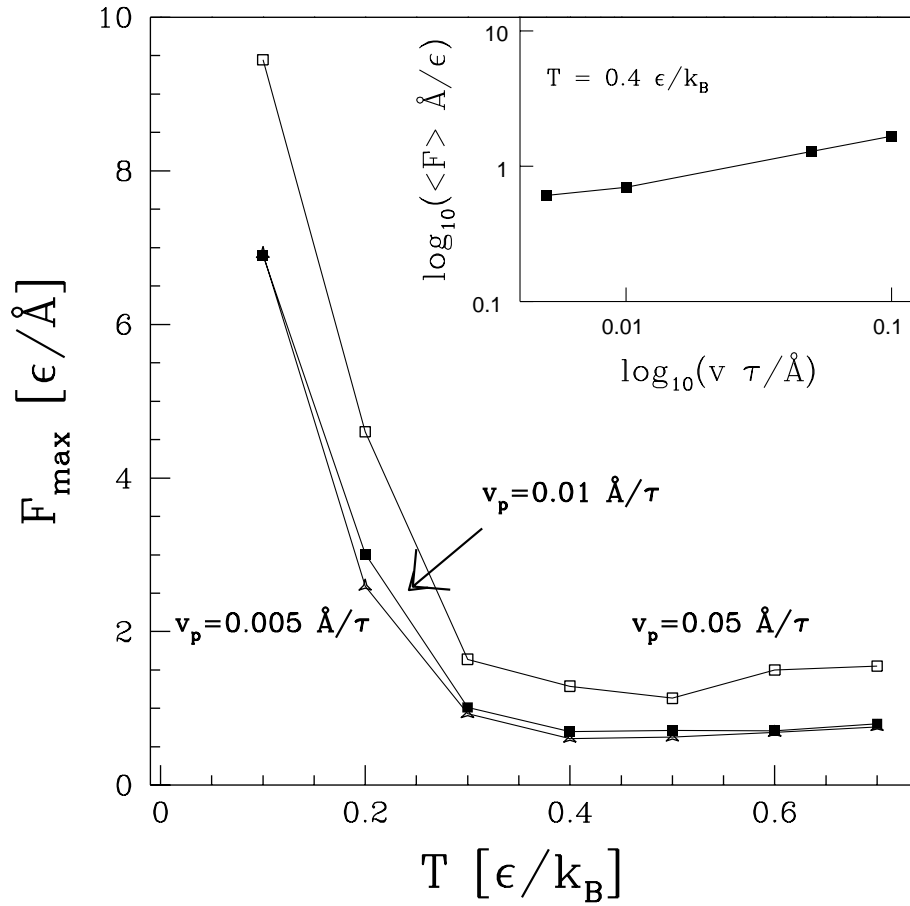


Figure 12: The C-type stretching in model I. The main figure shows F_{max} as a function of T for three values of v_p . The inset shows the log-log plot of F_{max} vs. v_p .

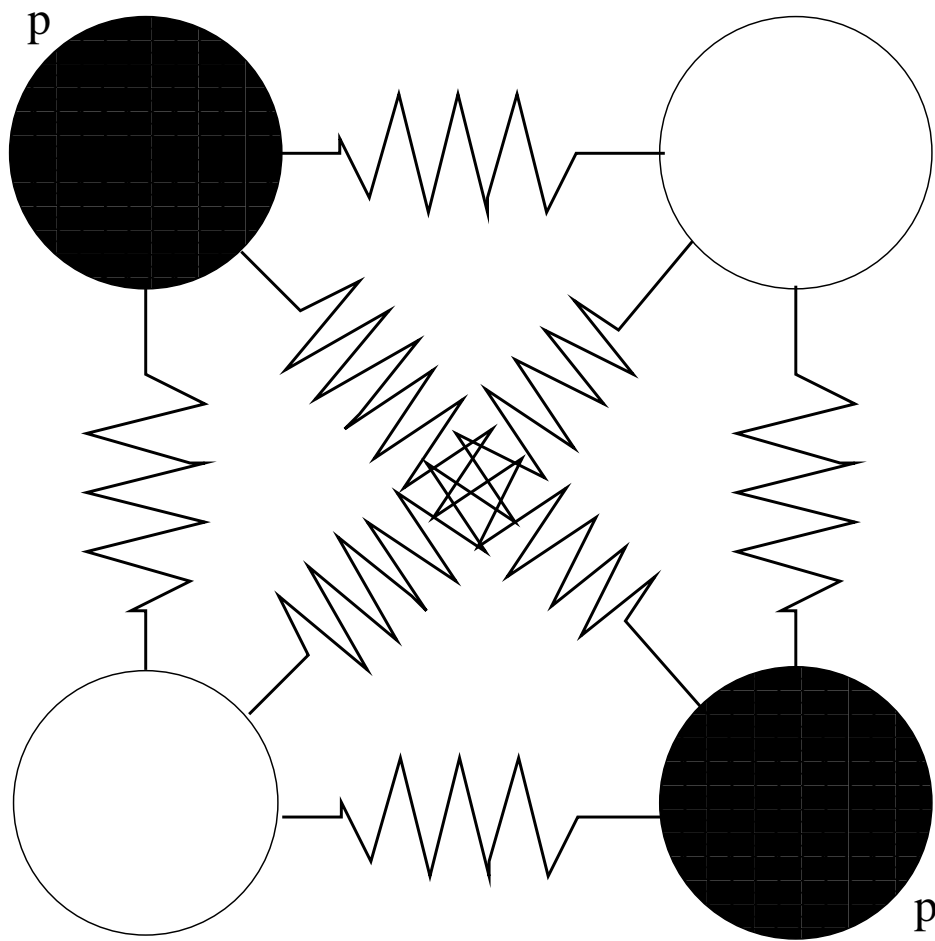


Figure 13: A schematic view of the beads mounted at the DNA end in order to apply torque through them. All beads are connected with the springs.

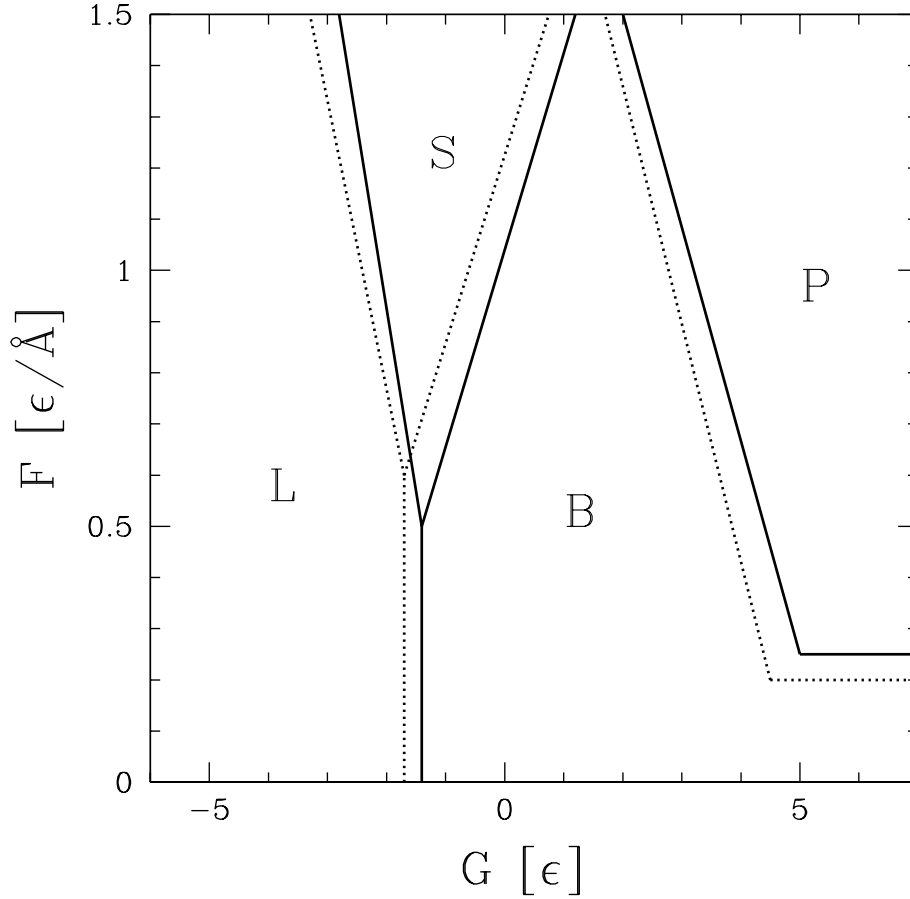


Figure 14: The phase diagram representing the final type of dsDNA structure obtained after applying the stretching force, F , and the torque, G , in model II. L denotes the L-DNA form, and S signifies stretched chains, in which the backbones form straight lines. B denotes the original B-type structure. P corresponds to the Pauling form of the DNA, where the backbones get closer to each other, and bases stay outside of the helix. The solid lines represent results obtained for $\tilde{T} = 0.4$, while the dashed ones for $\tilde{T} = 0.2$.

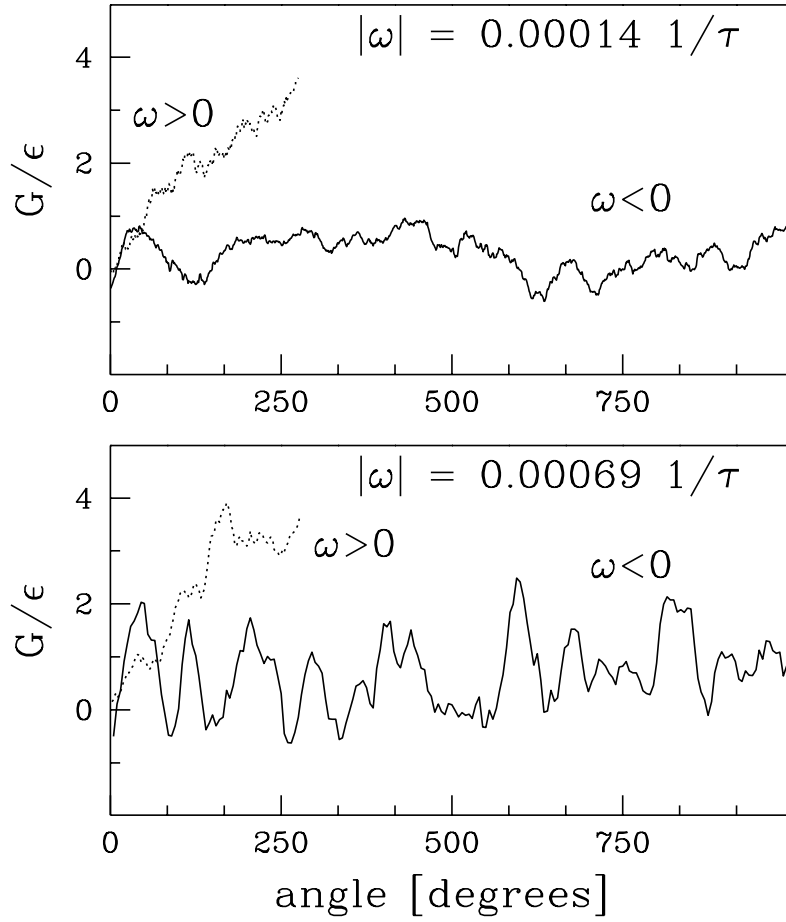


Figure 15: Torque of resistance to the twist as a function of the angle of rotation for two magnitudes of the angular velocities in $\tilde{T} = 0.4$ as indicated. The system consists of 20 base pairs and the simulations have been performed within model II. The dashed lines correspond to a sense of the twist that agrees with helical rotation of the dsDNA. The solid lines correspond to the opposite sense of the twist.